The Design of Independent Anchor Blocks for Vehicular-Impact Loadings

MALCOLM H. RAY

A simplified method for the analysis and design of independent anchor blocks is presented. Independent anchor blocks are structures designed to provide adequate guardrail-system anchorage and still remain independent of the bridge rail structure in guardrail–bridge rail transitions. Critical loadings for independent anchor blocks are discussed as well as the dynamic ultimate strength of soils. Equations of motion are developed from dynamic equilibrium considerations, and design curves are developed that can assist the designer in selecting the most appropriate geometry. Given the length and width of a particular independent anchor block, the design curves indicate what minimum embedment depth is required to minimize deflections in the critical-loading cases. Finally, the results of two full-scale crash tests are presented that verify the design curves.

The purpose of using independent anchor blocks in guardrail–bridge rail transitions is to provide a nearly rigid fixed support for the approach guardrail that remains independent of the bridge structure. This is generally accomplished by anchoring the guardrail system with a large mass. A simple method is presented for analyzing and designing independent anchor blocks in terms of providing anchorage and minimizing the anchor-block deflections.

Anchor blocks designed using traditional soil mechanics tend to be grossly overdesigned, which results in uneconomical designs. Traditional soil mechanics does not account for the increased strength of soils under dynamic conditions. As a result, most real-world anchor-block details are designed with little supporting methodology. In this paper an attempt is made to provide a simple method for designing such structures.

There are two distinct types of loadings that typically occur during a vehicle impact with an anchored approach guardrail; these two scenarios are shown in Figure 1. Case 1 represents a loading condition in which lateral overturning forces are transmitted to the anchor block in addition to longitudinal sliding forces. In this case, the block rotates about an axis parallel to the traveled way, which primarily results in shear failure in the soil behind the independent block as the base "kicks out." In Case 2, the vehicle strikes downstream of the anchorage, and the anchor block must resist the tensile force transmitted by the guardrail beam, which causes the block to slide through the soil being pulled by the guardrail beam. This loading results in a bearing failure on the narrow edge of the block.

A force-time history of an independent anchor block derived from a BARRIER VII *(1)* simulation is shown in Figure 2. The solid lines represent an idealized force-time history; the data points are the BARRIER VII estimates of the force at each time step. Using these idealized force-time histories and the two worst-case scenarios shown in Figure 1, the following sections will present a simplified independent anchor-block analysis procedure and a set of design curves to be used for selecting the footing width, embedment depth, and wall length required to ensure adequate independent anchor-block performance.

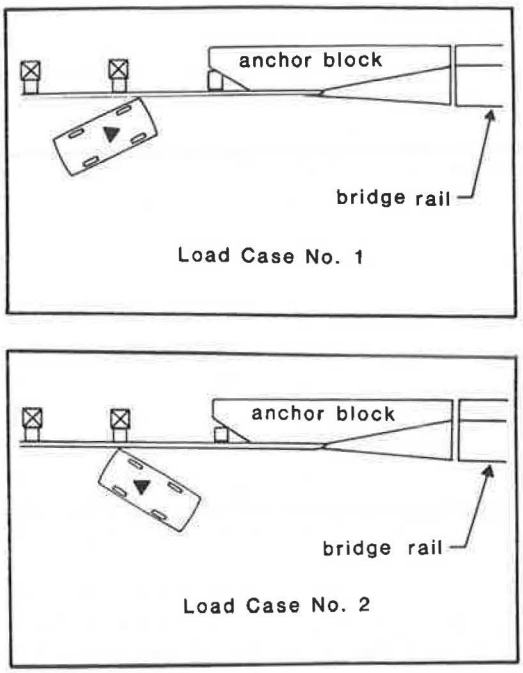

FIGURE 1 Critical load cases for an independent anchor block.

STRENGTH OF DYNAMICALLY LOADED SOILS

Ultimate Strength of Soils

The behavior of soils during dynamic large-deflection events is difficult to model. Soil is a highly nonlinear material; it is not homogeneous, it is nonisotropic, and its strength depends on many factors over which the designer has no knowledge or control. Except with small deflections, soils behave plastically and not elastically. There is therefore some ultimate plastic load with which the soil will resist motion regardless of the magnitude of the deflection. Figure 3 shows force-deflection plots of

Southwest Research Institute, San Antonio, Tex. 78284. Current affiliation: Box 1708, Station B, Vanderbilt University, Nashville, Tenn. 37235.

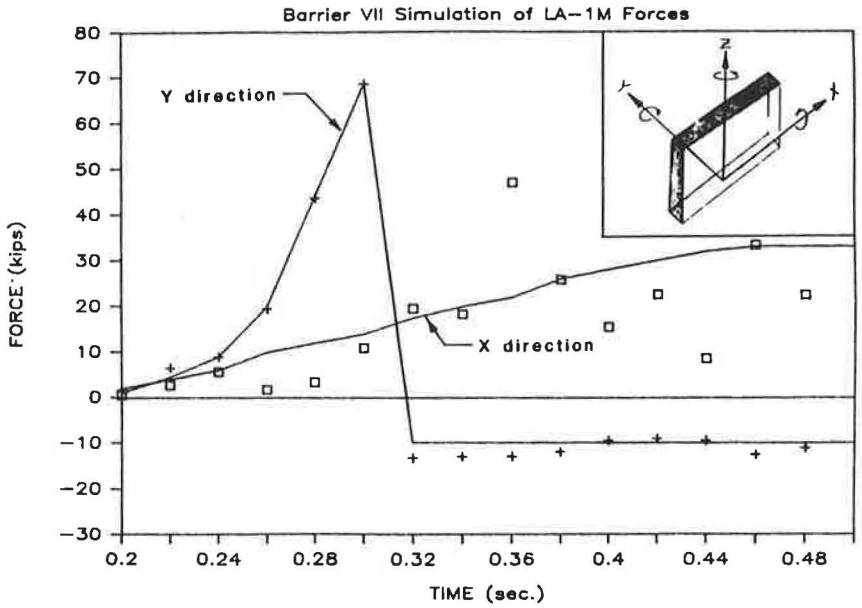

FIGURE 2 Idealized wall force-time history.

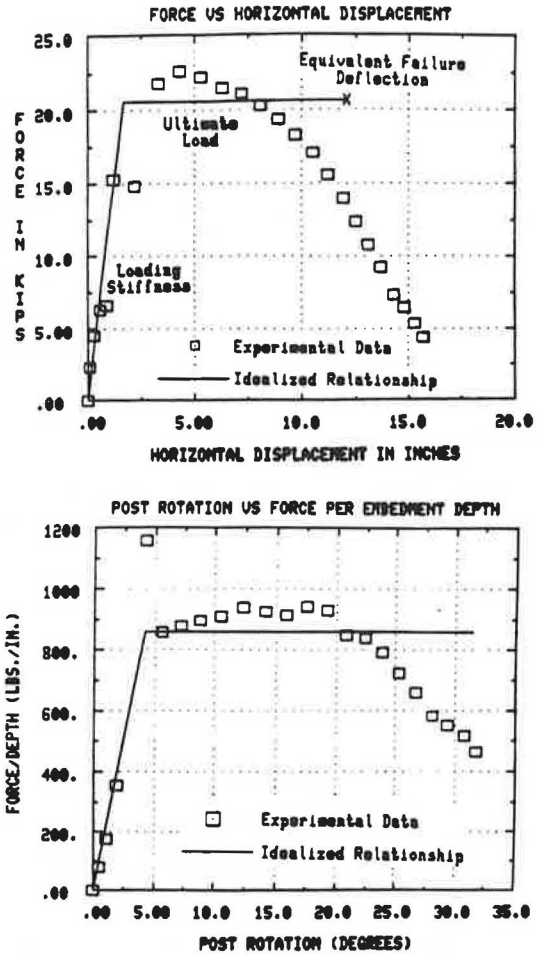

FIGURE 3 Force-displacement behavior of a dynamically loaded guardrail post embedded 44 in. into the soil *(4)*.

a guardrail post that illustrate the plastic behavior of soils when subjected to dynamic forces *(2)*. For both rotational and translational deflections, the soil behaves elastically for only 10 percent of the total deflection; the remaining 90 percent of the deflection exhibits plastic behavior.

The force drops below the ultimate value in the upper graph of Figure 3 for several reasons. First, as the post rotates, it is also being pulled from the ground, so that less soil is in contact with the post. Second, according to the Coulomb earth pressure theory *(3)*, the lateral earth pressure decreases as the rotation increases. If rotations, in the case of Figure 3, are less than 20 degrees, the idealized constant ultimate load will provide a good estimate of the soil strength. Because the purpose of the following procedure is to assist designers of independent blocks, the idealized ultimate soil resistance was used so that the deflections would not be excessive. Good performance was therefore defined as response that minimized block deflections. In the range of deflections acceptable to the designer, the ultimate resistance is nearly constant, that is, perfectly plastic.

The assumption that the ultimate soil strength is perfectly plastic greatly simplifies developing equations of motion for the independent anchor block. The anchor block must satisfy dynamic equilibrium at each time step; the applied forces, resisting forces, and inertial forces must all sum to zero. The acceleration acting on the block during any time step is therefore merely the sum of the resisting and applied forces divided by the applicable mass property of the block. The equations of motion will be developed fully in the next section.

Lateral Earth Pressure

Determining the lateral-earth-pressure coefficient is critical in determining the ultimate strength of soils. Terzaghi presents the following classical expression for lateral earth pressure *(4)*:

$$P_d = \gamma d (K_p - K_a) \quad (1)$$

where

P_d = lateral earth pressure,
γ = unit weight of soil,
d = depth of interest,
K_p = passive-earth-pressure coefficient, and
K_a = active-earth-pressure coefficient.

The Coulomb formulation *(3)* of the active and passive earth pressures was used in this analysis because it incorporates the rotation of the wall as well as the angle of internal friction, angle of wall–soil friction, and the slope of the backfill. For soils with large angles of internal friction (ϕ), the passive earth pressure (K_p) is much larger than the active earth pressure (K_a). Well-graded base materials that are typically used as the foundation for road surfaces generally have internal friction angles between 40 and 53 degrees. The term K_a therefore can be neglected for most practical design cases because it is very small compared with K_p. The Coulomb formulation of the passive pressure as presented by Bowles *(3)* is

$$K_p = \frac{\sin^2(\alpha + \phi)}{\sin^2\alpha \sin(\alpha + \delta)\left\{1 - \left[\frac{\sin(\phi + \beta)\sin(\phi + \delta)}{\sin(\alpha + \beta)\sin(\alpha + \delta)}\right]^{1/2}\right\}^2} \quad (2)$$

where

α = wall rotation,
δ = angle of wall–soil friction,
ϕ = angle of internal friction, and
β = slope of the backfill.

Unfortunately, the soil strength estimated using this form of K_p is much too low for dynamically loaded soils; predictions made using the Coulomb formulation are not at all accurate when compared with full-scale tests. When subjected to dynamic loads, soil appears to exhibit much greater strength. There are several possible reasons. First, because the event happens quickly, the soil moisture has no time to drain. This hydrodynamic resistance arises because the water cannot be pushed through the soil pores quickly enough; the end effect is to create miniature hydraulic cylinders that resist the dynamically applied load. A more important effect, especially in well-drained soils in which there is little water present, is interparticle friction. In static tests, soil particles will align themselves and flow slowly. During dynamic events, the particles are not aligned and cannot flow as quickly because of higher interparticle friction. One reason for specifying well-graded base materials for roadway construction is to provide a wide range of particle sizes, which will ensure a high degree of interparticle friction.

Although soil behavior is easily rationalized, it is far more difficult to quantify its effects. Dewey et al. *(5)* reported on a number of static and dynamic tests of guardrail posts embedded in soil. By comparing the magnitudes of the ultimate loads observed in static and dynamic tests, it was observed that soils, or at least well-graded crushed gravel, were approximately 5 times stronger during dynamic events than during static events. The lateral passive-earth-pressure coefficient in the following analysis was therefore multiplied by a factor of 5 to provide a more realistic though wholly empirical estimate of the lateral soil strength.

The final and perhaps most critical factor in estimating lateral soil strength is the shape of the soil pressure distribution. Figure 4 shows a distribution empirically derived by Seiler *(6)* for laterally loaded timber poles. The choice of the pressure distribution shape will define the point of rotation.

ANALYSIS OF THE INDEPENDENT BLOCK

Dynamic Equilibrium

Because dynamic equilibrium must be satisfied at each time step, a short 200-line BASIC program called the Independent Block Analysis Program (IBAP) was written to solve the large number of repetitive equations quickly. In the following sections the derivation of the equations used in the simple analysis program is presented.

The first step in writing equations of motion for the independent block is to calculate the resultant acceleration for each degree of freedom (df). At each time step, the sum of the applied and resisting forces must be equal to the acceleration of the block for dynamic equilibrium or

$$P_{an} + P_{rn} = \frac{A_n}{I_n} \quad (3)$$

where

P_{an} = applied load in the df n-direction,
P_{rn} = resistance in the df n-direction,
A_n = acceleration in the df n-direction,
I_n = inertial property of the block for the nth df, and
n = df from 1 through 6.

Translation

Referring to Seiler's pressure distribution in Figure 4, the following equations can be written for the x and y translational df's:

$$A_x M = P_{ax} - R_{1x} + R_{2x} - \mu W_b \tan\phi$$

where

A_x = acceleration in the x-direction,
M = mass of the block,
μ = coefficient of soil–block friction,
W_b = weight of the anchor block, and
P_{ax} = applied load in the x-direction.

The third term represents the contribution of base friction to the total resistance. Recognizing that the distribution in Figure 4 is parabolic, expressions for soil resistance R_1 and R_2 can be rewritten as follows:

$$R_1 = \left(\frac{4}{3}\right)\left(\frac{DB}{3}\right)P_d = \frac{4DBP_d}{9}$$

By integrating the expression for the soil pressure distribution shown in Figure 4 between $0.67D$ and D, an expression for the force R_2 can be developed as follows:

$$R_2 = \gamma K_p \int_{0.68D}^{D} \frac{-2.9}{D} d^2 + 1.97d\, dd$$

$$= \gamma K_p \left(\frac{-2.9}{3D} d^3 + \frac{1.97}{2} d^2\right)_{0.68D}^{D}$$

$$= 0.134\gamma K_p D^2$$

where

B = width of block,
D = embedment depth, and
P_d = maximum lateral earth pressure.

Using Equation 1 to calculate P_d at a depth of $D/3$ yields the following:

$$P_d = 0.333\gamma DK_p$$
$$R_1 = 0.148\gamma D^2 BK_p$$
$$R_2 = 0.134\gamma D^2 BK_p \quad (4)$$

where γ is the unit weight of the soil. The x-direction and the analogous y-direction resistances to translation are therefore found to be

$$A_x M = P_{ax} - 0.014\gamma D^2 BK_p - \mu W_b \tan\phi$$
$$A_y M = P_{ay} - 0.014\gamma D^2 LK_p + \mu W_b \tan\phi \quad (5)$$

where L is block length.

The sign of the base friction term in Equations 5 is due to an assumption about how the block is likely to deflect. Because the length will be much greater than the width, base friction will have the same sense as the applied load for the y-direction because base friction will resist overturning and the opposite sign for the x-direction because pitch rotation is unlikely and friction will oppose the x-translation. It was assumed that displacement in the z-direction was negligible. The acceleration, therefore, in the z-direction was always set to zero.

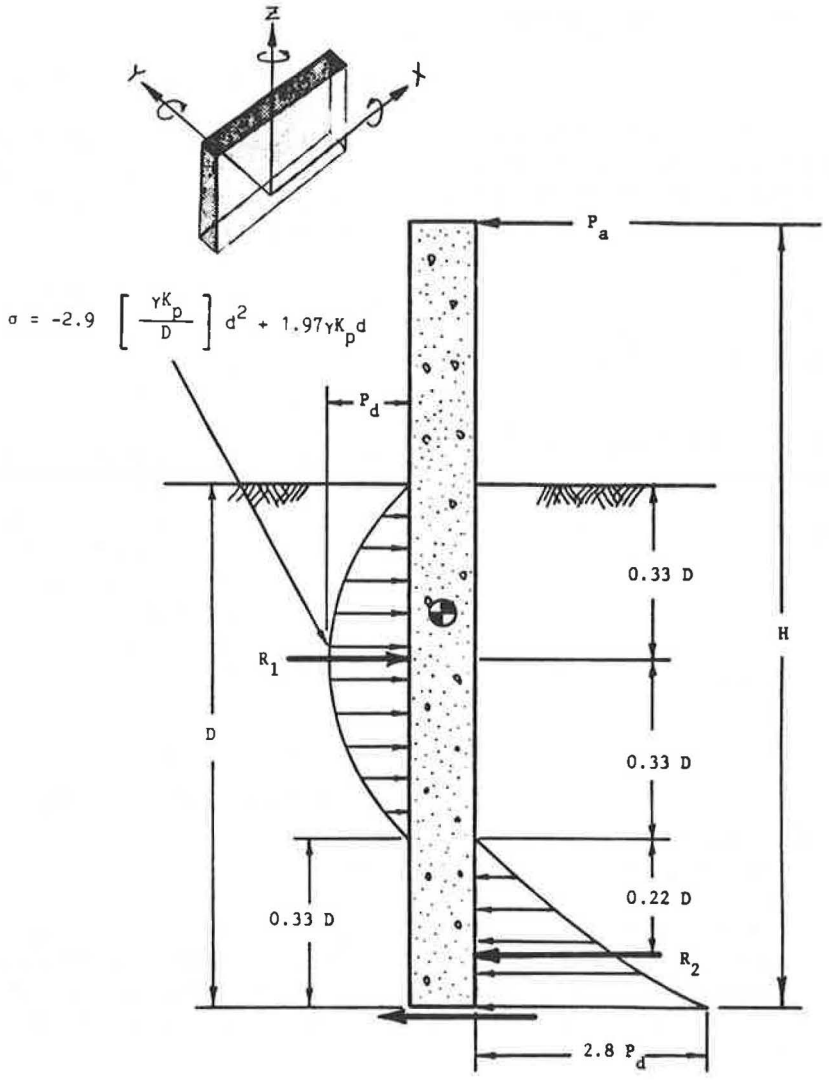

FIGURE 4 Seiler's lateral soil pressure distribution *(6)*.

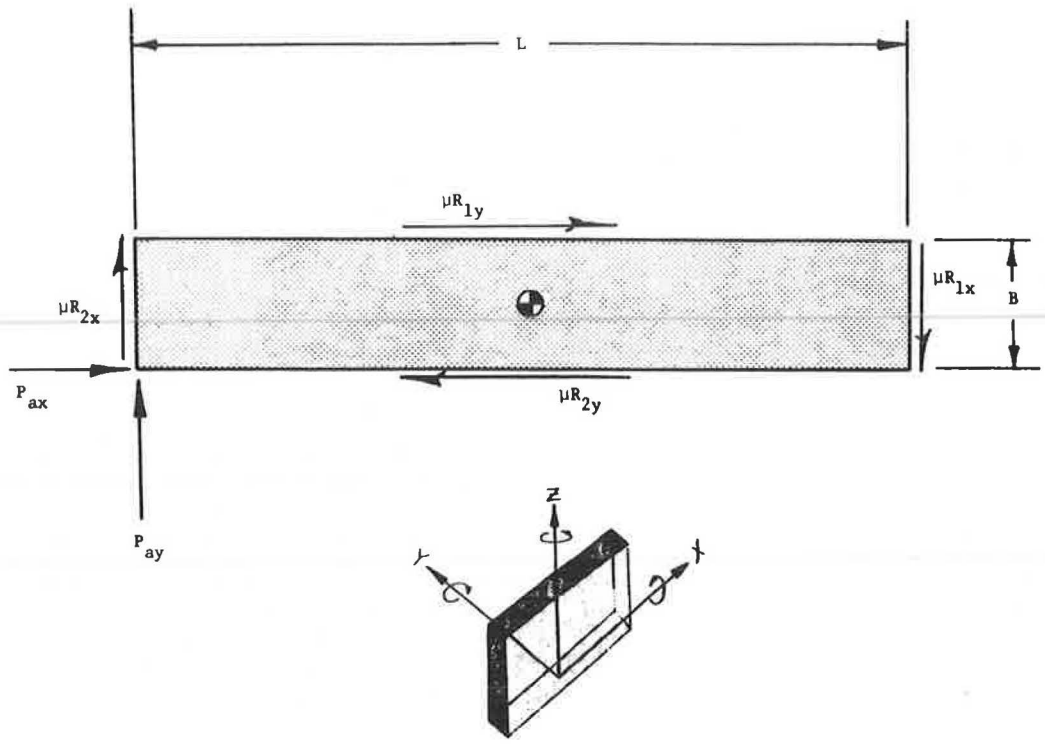

FIGURE 5 Forces resisting yaw rotation.

Rotations

Rotation about the x-axis is called roll and rotation about the y-axis is called pitch. Again, the equations are analogous for both x- and y-rotations. Figure 4 shows the moments that resist rotations of the anchor block.

$$A_{\text{roll}}I_{xx} = \frac{1}{2}P_{ay}H + R_1\left(\frac{H}{2} - \frac{2D}{3}\right) - R_2\left(\frac{H}{2} - \frac{D}{4.5}\right) - \mu W_b \tan\phi\left(\frac{H}{2}\right)$$

Substituting Equations 4 into the foregoing expression and simplifying yields

$$A_{\text{roll}}I_{xx} = \frac{1}{2}P_{ay}H + \gamma D^2 L K_p\,(0.007H - 0.070D) - \frac{1}{2}W_b H\mu\tan\phi$$

$$A_{\text{pitch}}I_{yy} = \frac{1}{2}P_{ax}H + \gamma D^2 B K_p\,(0.007H - 0.070D) - \frac{1}{2}W_b H\mu\tan\phi \quad (6)$$

Yaw is not a primary mode of displacement because the overturning and sliding strength are generally much less. In loading Case 2, yaw rotation is ignored because the guardrail beam is attached near the y-z center of gravity, and the moment arm is therefore very small. For load Case 2, yaw is more likely to occur although it is conservative to ignore it because the bridge rail end of the anchor block will rotate into the traveled way where it will shield the vehicle from snagging on the bridge rail. Yaw rotation was included in this analysis only for loading Case 1.

Yaw resistance arises mainly from frictional forces acting on the bearing surfaces of the block. Referring to Figure 5, the resisting force and the applied force produce the following yaw acceleration:

$$A_{\text{yaw}}I_{zz} = \frac{P_{ax}B}{2} - \frac{P_{ay}L}{2} - \frac{\gamma D^2 K_p BL}{4} \quad (7)$$

Equations of Block Motion

With the foregoing equations representing the block's acceleration at any time step, the derivation of the block's equations of motion is straightforward. At each time increment, the applied load is estimated from the BARRIER VII simulation shown in Figure 2 and read from an external file and the acceleration terms are calculated with Equations 5 through 7. The velocity and displacement of each degree of freedom are given by the following equations:

$$V_{i,n} = V_{i-1,n} + A_{i,n}\Delta t \quad (8)$$

$$\Delta_{i,n} = \Delta_{i-1,n} + 0.5\,(V_{i-1,n} + V_{i,n})\,\Delta t \quad (9)$$

where

$V_{i,n}$ = velocity of block at time i for df n,
$A_{i,n}$ = acceleration of block at time i for df n,
$\Delta_{i,n}$ = displacement of block at time i and df n,
Δt = time increment, and
i = time step number.

The acceleration, velocity, and displacement of each of the block's degrees of freedom can be easily calculated by starting at time zero and working incrementally through the last time step.

DESIGN OF INDEPENDENT ANCHOR BLOCKS

Using the analysis method presented in the previous section as implemented in IBAP, a set of curves was formulated to assist the designer in quickly selecting the wall length, footing width, and embedment depth required to minimize deflections. The idealized loadings represented in Figure 1 were used to simulate Case 1 and Case 2 loadings.

In order to develop strength, soils must experience some deformation. The curves of Figures 6 and 7 were derived by finding the footing width required to prevent excessive deflection for a given wall length and embedment depth. A width was deemed adequate when the deflection at the point of the most extreme corner of the block was less than 1 in. (2.54 cm), which was chosen as a critical displacement because deflections of more than 1 in. could produce snag points from nonalignment of the faces of the independent anchor block and the bridge structure. The vehicle, after causing the wall to rotate, could snag on the end of the rigid bridge rail.

In order to generate fairly generic design curves, it was necessary to assume some typical or at least conservative geometry. The geometry chosen is shown in the inset to Figures 6 and 7. Most typical wingwalls would perform somewhat better because they use a sloped wall, which adds more weight, thus increasing the inertial resistance of the block.

The solid lines in Figure 6 show the family of curves for load Cases 1 and 2. Each curve corresponds to a particular embedment depth and can be used to select the most appropriate footing width. For example, if an anchor wall 18 ft (54.8 m) long with a footing width of 20 in. (50.8 cm) is to be used, Figure 6 indicates that the embedment depth must be at least 24 in. (61 cm) to prevent excessive roll rotation after a load Case 1 impact.

Load Case 2, in which the anchor block slides in the x-direction, is also represented in Figure 6. For example, the 18-ft-long, 20-in.-wide wall that was adequate for Case 1 is also adequate for this loading, though more marginal than for Case 1.

If the solid and dashed lines in Figure 6 are compared, it becomes apparent that load Cases 1 and 2 can both be critical for different geometries. Figure 7 is a set of curves that show only the critical values. In the portion of Figure 7 below the dashed lined, sliding stability dominates and load Case 2 controls. In the area above the dashed line, overturning stability is critical and load Case 1 controls. With Figure 7, the designer merely needs to select the embedment depth represented by the curved line just below the plotted point defined by the wall length and footing width.

FULL-SCALE CRASH TESTS

Two independent-anchor-block designs were tested in this research program—one state standard and one designed according to the design curves shown in Figure 6.

Standard Design Test

The standard design tested was a G4(2W) guardrail transition to an 18-ft-long independent block embedded 10 in. into the soil. The footing width of the independent block was 1 ft 8.5 in., as shown in Figure 8. Referring to the design curves in Figure 7, the embedment depth required to provide adequate performance given the length and width of the block should have been 24 in. and not 10 in. Figure 9 shows the test installation before the collision.

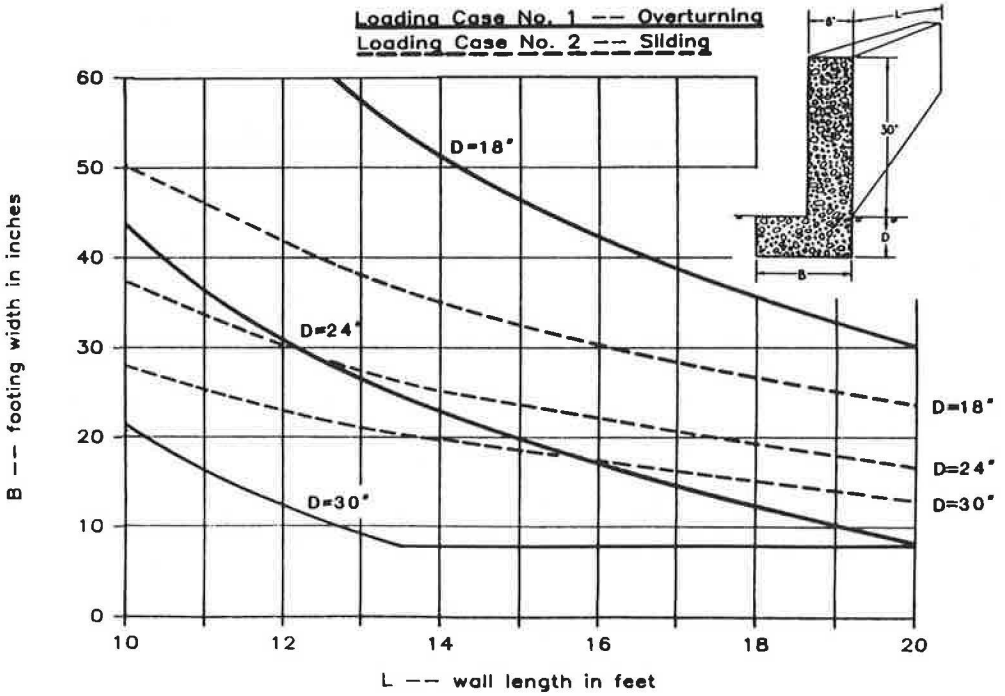

FIGURE 6 Design curves for load Cases 1 (overturning) and 2 (sliding).

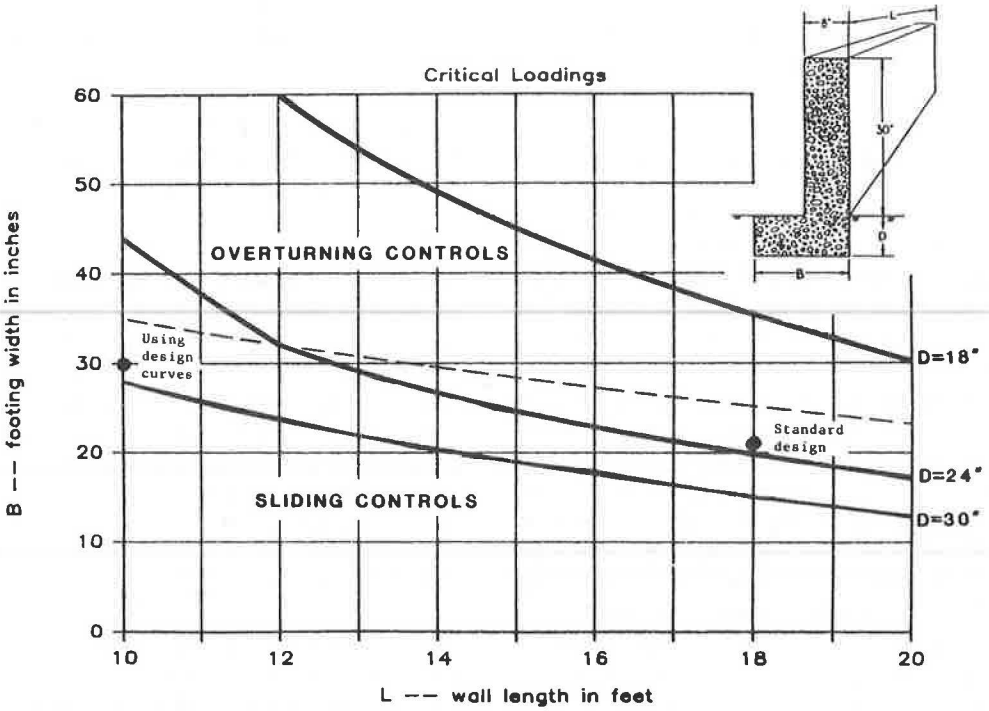

FIGURE 7 Design curves for the critical load case.

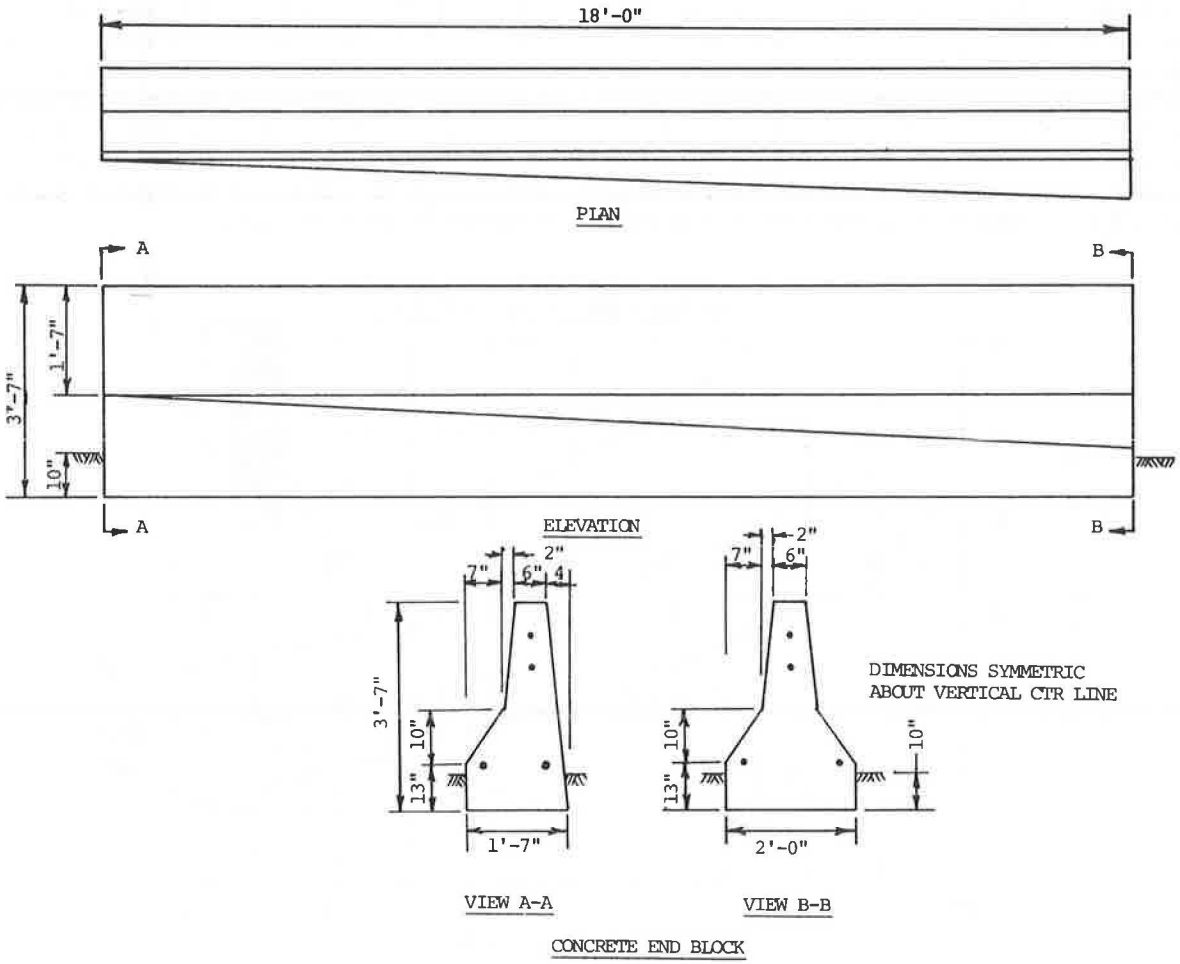

FIGURE 8 Standard independent anchor block design.

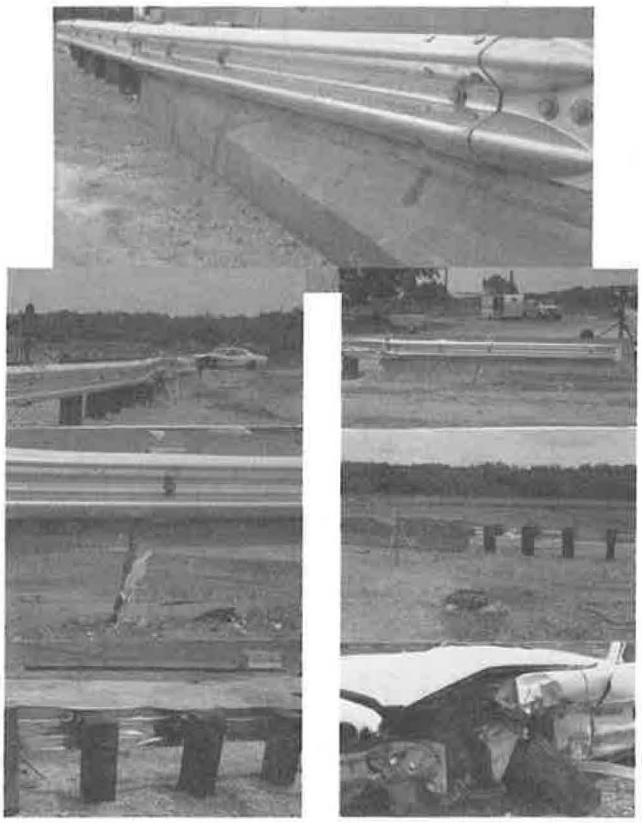

FIGURE 9 Standard design test photographs.

Although the 4,500-lb test car was redirected as shown in Figure 10, the vehicle experienced severe snagging on the end of the independent end block. This snagging was due to the post spacing of 3 ft 1.5 in. near the end of the block. The block rolled considerably, greatly exceeding the arbitrary 1-in. maximum deflection selected in the previous sections. The block, as designed, did not have sufficient embedment to adequately resist the impact loading as predicted by the design curves in Figure 7. A test summary appears in Figure 11.

Modified Design

The modified independent anchor block tested was designed by using the design chart shown in Figure 7. The same flat wall tapered to a safety shape was used as that in the standard design test. The primary difference between these two tests was the embedment depth, total block length, and the footing width. An 18-in.-wide footing was used that extended 30 in. below grade. The point represented by this geometry is shown in Figure 7. The selection of a 10-ft wall length necessitates using a footing 30-in. wide and an embedment 18-in. deep.

Post spacings in this transition were derived from other full-scale tests of transition systems. The modified-design test utilized a reduced post spacing of 3 ft 1.5 in. and 1 ft 6.75 in. near the upstream end of the independent block. This reduced post spacing and the addition of a lower rub rail are required to prevent the serious snagging observed in the standard-design test. The last 12-ft 6-in. section of W-beam was nested or

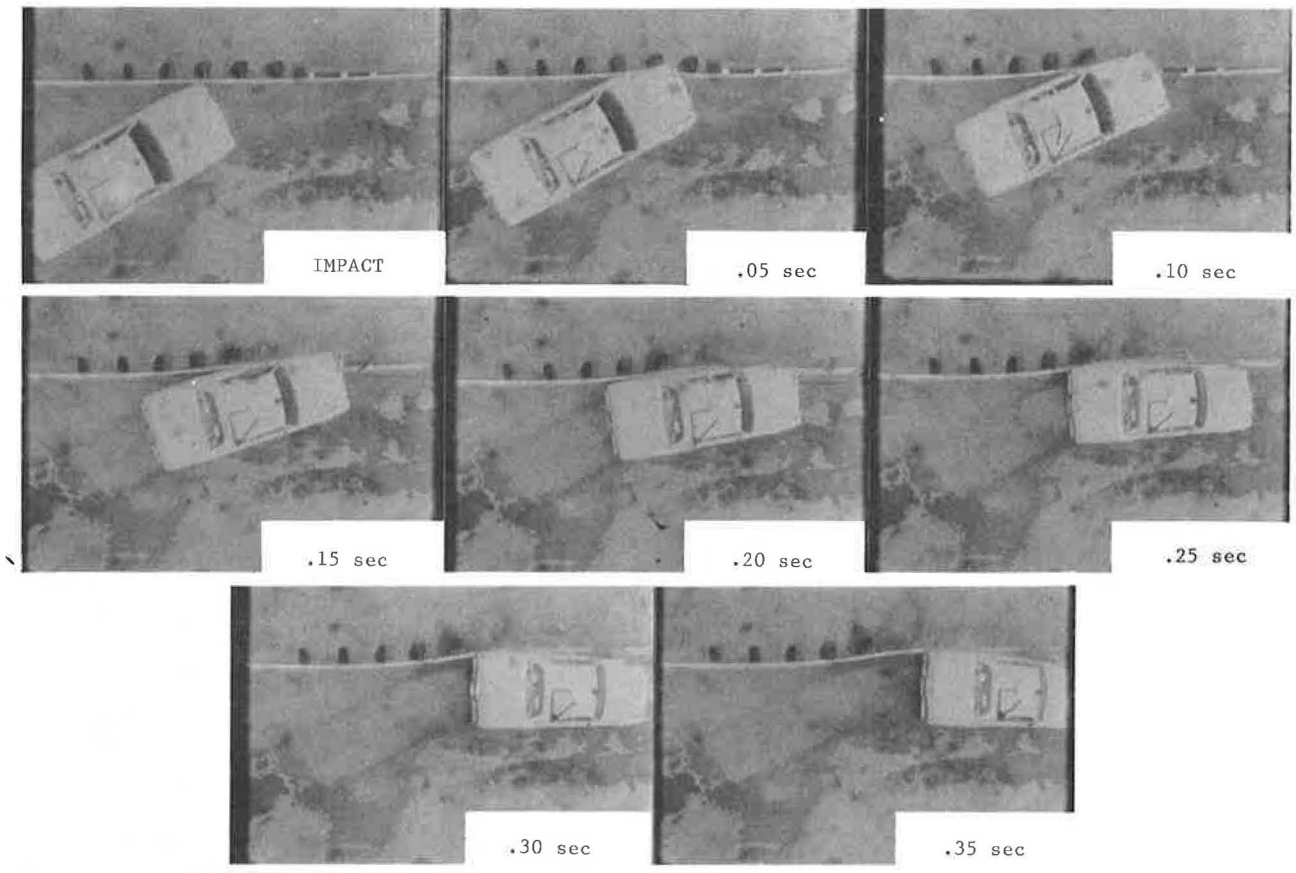

FIGURE 10 Sequential photographs of standard design.

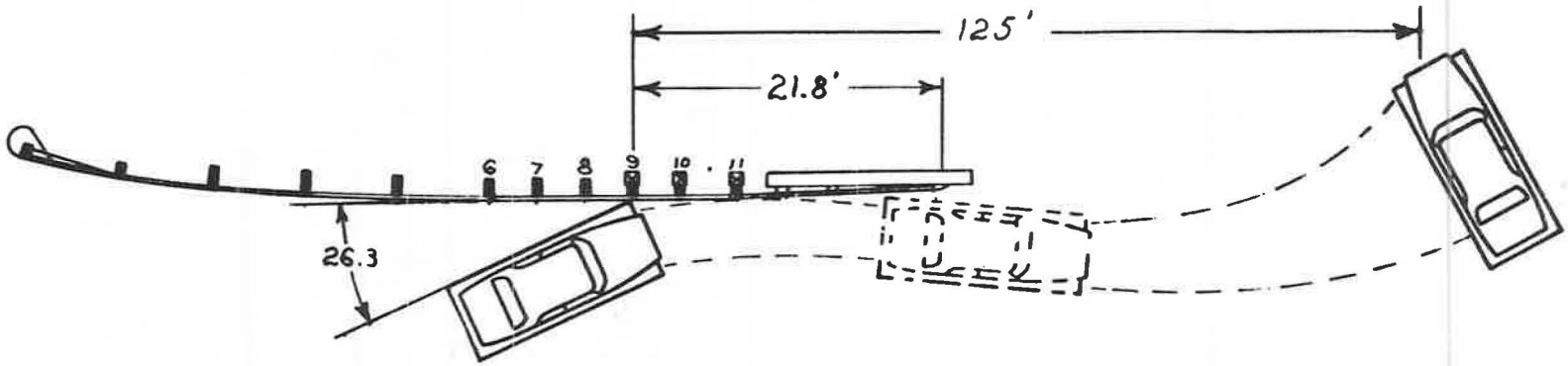

Test No. NV-1

Date 5-15-84

Installation Length - ft (m) 62.5 (19.1)

Beam

- Member ..... 12-ga. W-beam
- Length - ft (m) 12.5 (3.8)

Maximum Deflections

- Dynamic - in. (cm) 16.6 (42.2)
- Permanent - in. (m) 6.1 (15.5)

Posts 1 through 8

- Material ..... Wood
- Description - in. (cm) 6x8x64 (15x20x163)
- Embedment - in. (cm) 36 (91)
- Spacing - ft (m) ..... #1 thru 6, 6'-3" (1.9)
  #6 thru 11, 3'-1 1/2" (1.0)

Posts 9 through 11

- Material ..... Wood
- Description - in. (cm) 10x10x64 (25x25x163)
- Embedment - in. (mm) 36 (91)
- Spacing - in. (mm) 3-1 1/2 (1.0)

Soil Type and Condition ..... S1 (Dry)

Vehicle ..... 1978 Dodge Sedan

Mass - lb (kg)

- Test Inertia 4306 (1952)
- Dummies 330 (150)
- Gross 4636 (2102)

Speed - mph (kph)

- Impact 61.3 (98.6)
- Exit 35.1 (56.5)

Angle - deg

- Impact 26.3
- Exit ..... -7.1

Occupant Impact Velocity - fps (m/s)

- Forward (film/accel) ..... 24.8 (7.6)/18.0 (5.5)
- Lateral (film/accel) ..... 17.7 (5.4)/15.8 (4.8)

Occupant Ridedown Accelerations - g's

- Forward (film/accel) ..... -4.1/NA
- Lateral (film/accel) ..... -5.3/NA

Maximum 50 msec Avg Accelerations - g's

- Longitudinal (film/accel) ..... -6.9/-9.9
- Lateral (film/accel) ..... -5.4/-7.9

Damage

- TAD 11-FL-7
- VDI 12FDEW9

FIGURE 11 Summary of standard design test.

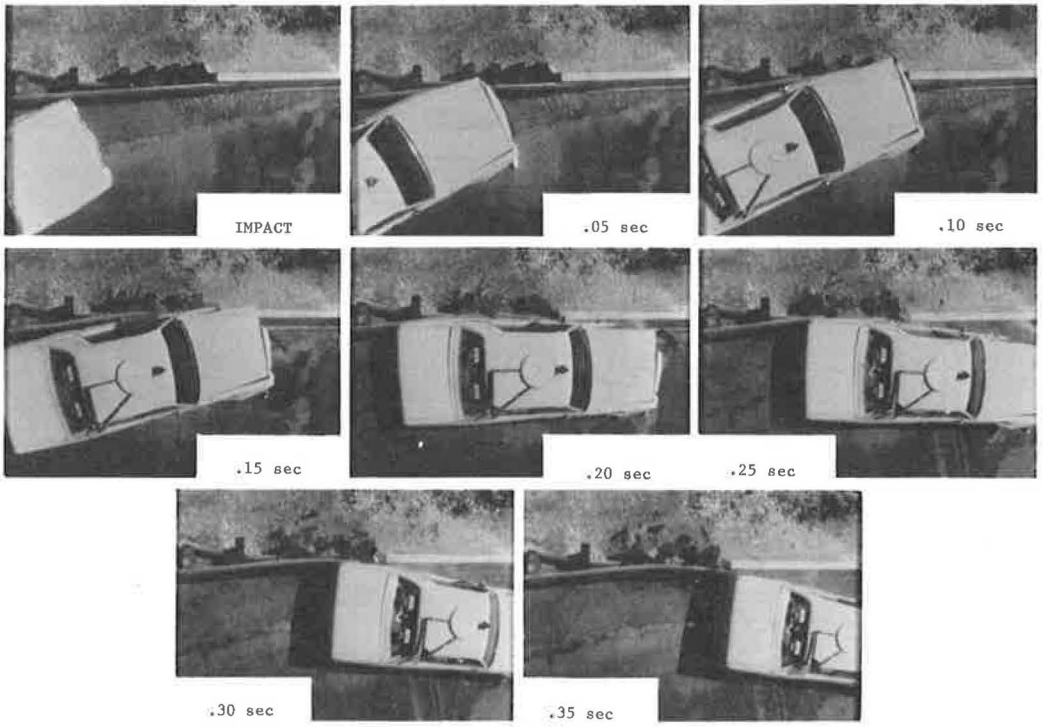

FIGURE 14 Sequential photographs, modified design test.

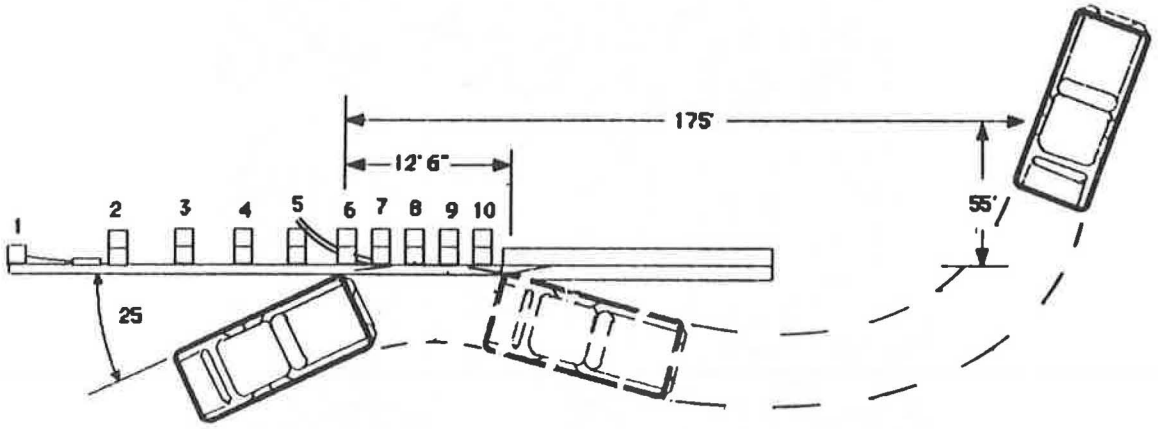

Test No. IB-1

Date 3-19-86

Installation Length - ft (m) 60 (18)

Beam
- Member ..... 12-ga. W-beam
- Length - ft (m) ..... 12.5 (3.8)1
- Rub rail ..... 12.5 (3.8) 12-ga. W-beam

Maximum Deflections - in (cm)
- Dynamic 10.5 (26.7)
- Permanent 5.3 (13.5)

Post
- Material ..... Wood
- Description ..... 6"x8"x72" (15 cm x 20 cm x 1.8 m)
- Embedment - in. (m) 44 (1.1)
- Spacing - ft (m) ..... #1 thru 4, 6'-3" (1.9)
- ..... #4 thru 6, 3'-1 1/2" (0.9)
- ..... #6 thru 3, 1'-6 3/4" (0.5)

Soil Type and Condition ..... S1 (Dry)

Vehicle ..... 1978 Plymouth

Mass - lb (kg)
- Test Inertia 4420 (2004)
- Dummies 330 (150)
- Gross 4750 (2154)

Speed - mph (km/h)
- Impact 60.1 (96.7)
- Exit 43.2 (69.4)

Angle - degree
- Impact 24.4
- Exit ..... -11.4

Occupant Impact Velocity - fps (ms)
- Forward (film/accel) ..... 3.0 (0.9)/19.3 (5.9)
- Lateral (film/accel) ..... 21.7 (6.6)/21.0 (6.4)

Occupant Ridedown Accelerations - g's
- Forward (accel) 5.1
- Lateral (accel) ..... -18.6

Maximum 50 ms Avg Accelerations - g's
- Longitudinal (film/accel) ..... -5.4/-10.6
- Lateral (film/accel) ..... -8.6/-10.2

Damage
- TAD 11-FL-6
- VDI 11FLEW6

FIGURE 15 Summary of modified design test.

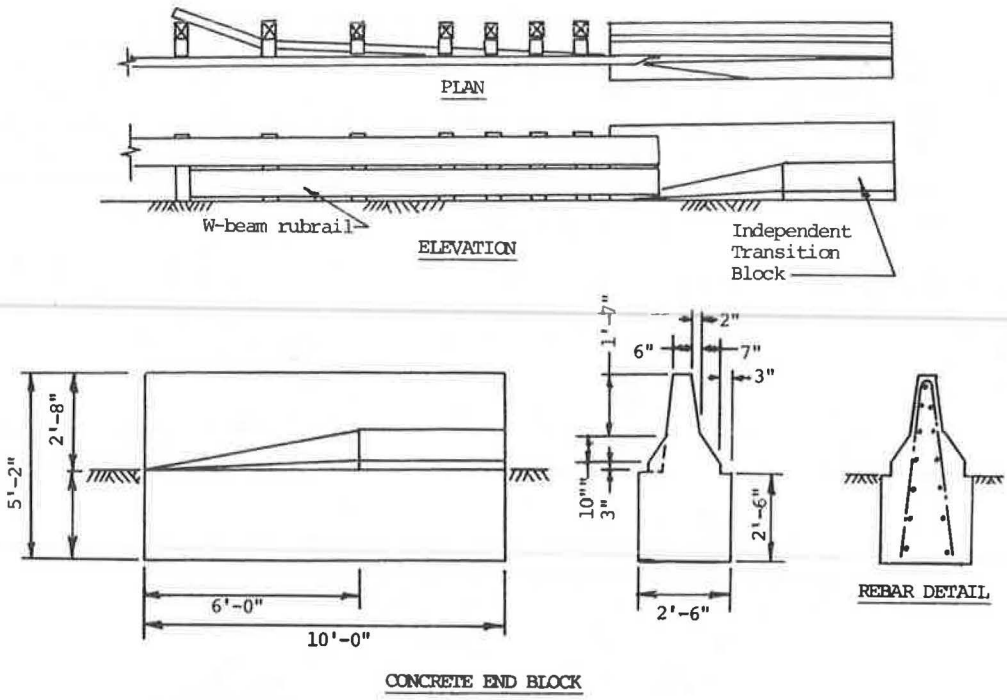

FIGURE 12 Modified independent anchor block design.

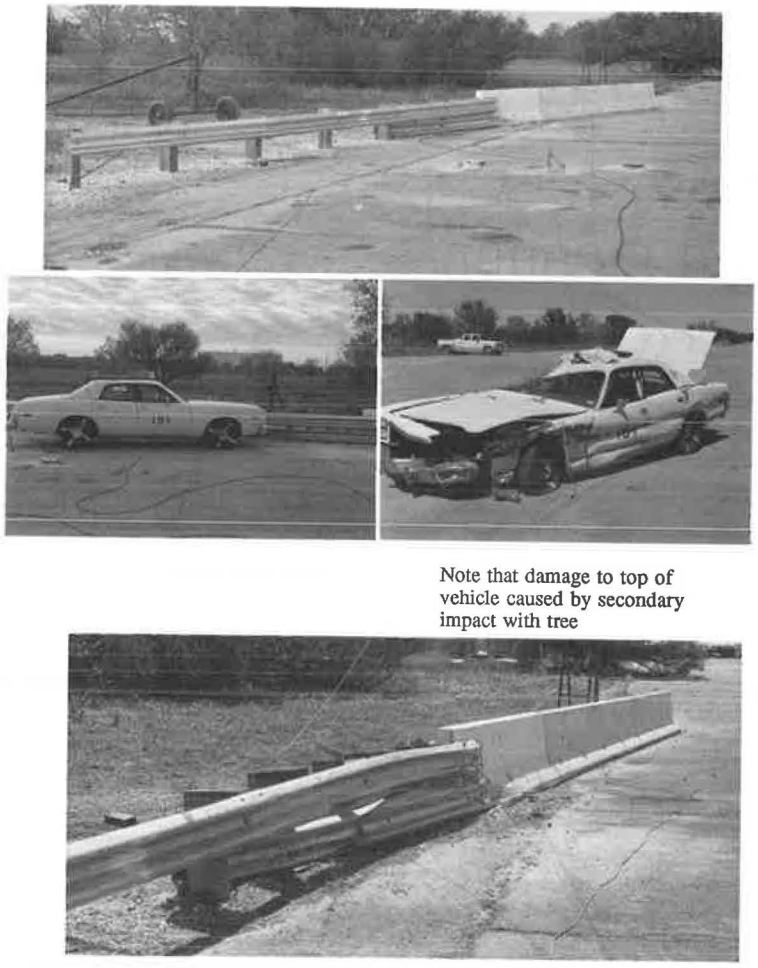

Note that damage to top of vehicle caused by secondary impact with tree

FIGURE 13 Before-and-after photographs, modified design test.

doubled in the modified design, which is shown in Figure 12. Before-and-after views of the test installation are shown in Figure 13.

The 4,500-lb car was smoothly redirected, as shown in Figure 14. A summary of the modified design test is shown in Figure 15. The independent anchor block experienced no displacement during the test; thus the curves of Figure 7 provided a suitable design.

SUMMARY

When conventional soil-strength analysis is used, the geometry required to provide adequate support against displacements of the anchor wall is far too conservative in comparison with designs that have been shown to perform well in the field. In the previous sections a simple method of modifying traditional soil-strength analysis techniques has been outlined that will produce far more realistic designs. The first modification required was to account for the increased strength of soils under dynamic loadings. This was done by multiplying the usual Coulomb passive-earth-pressure coefficient by an empirically observed factor of 5. A second modification was to enforce dynamic instead of static equilibrium in calculating the forces acting on the block. Using an incremental time step and an assumed force-time history allowed the calculation of the acceleration, velocity, and displacement of the block at each time step. With the resulting design curves, the designer can determine the geometry required to ensure good performance of independent anchor blocks.

ACKNOWLEDGMENTS

This work was sponsored by the Federal Highway Administration in the project Guardrail–Bridge Rail Transition Designs. The author would like to thank Charles McDevitt, the FHWA technical representative, for his guidance in this research. The author is also indebted to Maurice Bronstad and Lee Calcote, the coprincipal investigators, for their invaluable assistance, comments, and guidance during this research. The author would also like to thank Loretta Mesa for her efforts in the drafts and revisions of this paper.

REFERENCES

1. G. H. Powell. *BARRIER VII: A Computer Program for Evaluation of Automobile Barrier Systems*. FHWA-RD-73-51. FHWA, U.S. Department of Transportation, April 1973.
2. J. D. Michie, M. H. Ray, and W. N. Hunter. *Evaluation of Design Analysis Procedures and Acceptance Criteria for Roadside Hardware*. Final Report. Southwest Research Institute, San Antonio, Tex., 1986.
3. J. Bowles. *Foundation Analysis and Design*, 3rd ed. McGraw-Hill, New York, 1982.
4. K. Terzaghi. *Theoretical Soil Mechanics*. John Wiley and Sons, Inc., New York, 1943.
5. J. F. Dewey, J. K. Jeyapalan, T. J. Hirsch, and H. E. Ross. *A Study of the Soil-Structure Interaction Behavior of Highway Guardrail Posts*. Technical Report FHWA/TX-84/23+343-1. Texas State Department of Highways and Public Transportation, Austin, Sept. 1982.
6. J. F. Seiler. Effect of Depth of Embedment on Pole Stability. *Wood Preserving News*, Vol. 10, No. 11, Nov. 1983, pp. 152–160.